ASCE

Experimental Cyclic Response of a Novel Friction Connection for Seismic Retrofitting of RC Buildings with CLT Panels

Francesco Boggian[1]; Carola Tardo[2]; Angelo Aloisio, M.ASCE[3]; Edoardo M. Marino[4]; and Roberto Tomasi[5]

Abstract: The seismic vulnerability of existing RC framed buildings in seismic-prone areas requires affordable and practice-oriented solutions for their retrofitting. In this paper, the authors present a retrofitting solution for RC buildings based on the combined use of cross-laminated timber (CLT) panels and asymmetric friction connections (AFCs). The AFC connection is activated when the force level reaches the design threshold. The energy dissipation of the AFC increases the structural dissipation capacity and reduces the displacement demand. This research presents the outcomes of an experimental campaign on selected prototypes of these AFC connectors. The authors assess their dissipative capacity from cyclic load tests in four different connector arrangements and examine the contribution of aluminum shim layers. The first results highlight the significant dissipation potential of the AFC, although they also provide evidence of the notable sensitivity on the design and constructive details. The authors present a modeling approach to simulate the experimental results. **DOI: [10.1061/(ASCE)ST.1943-541X.0003313](https://doi.org/10.1061/(ASCE)ST.1943-541X.0003313).** *This work is made available under the terms of the Creative Commons Attribution 4.0 International license, https://creativecommons.org/licenses/by/4.0/.*

Introduction

The seismic retrofitting of existing buildings is a comprehensive and contemporary research topic with diverse economic, social, and environmental entanglements. This paper is part of the European Energy and Seismic Affordable Renovation Solutions (e-SAFE) project (e-SAFE n.d.), which presents a multidisciplinary approach on renovation solutions for existing buildings, in the framework of the Horizon (2020) European goal. The authors focus on seismic retrofitting, which represents an all-embracing challenge, especially in earthquake-prone areas in southern Europe. As an example, 60% of Italian residential buildings were built between 1946 and 1990, while 25% were built before 1946 (Istat 2015). The Italian seismic hazard and the inadequacy of seismic provisions before the 1980s confirm the Italian territory's significant seismic risk. There are several solutions for seismic retrofitting of RC buildings. Specifically, there are two types of interventions, those aiming to reduce the seismic demand and those aiming to increase the structural capacity (Pantazopoulou et al. 2016; Di Ludovico et al. 2017; Caterino et al. 2008). The structural capacity may be increased by adopting strengthening interventions or by installing stiffening elements. So far the strengthening interventions are the most widespread. They can be traditional [e.g., steel jacketing of beams and columns (Dubey and Kumar 2016)] or based on the use of advanced materials [wrapping with fiber-reinforced polymers (FRPs) or textile-reinforced mortar (Del Vecchio et al. 2014; Bournas et al. 2009)]. Properly designed stiffening elements [e.g., RC shear walls, X-bracing (Rahimi and Maheri 2018, 2020)] could partially adsorb the seismic load. However, the seismic vulnerability could also be reduced by lessening the seismic demand. These interventions include the use of dissipation devices (Javadi et al. 2020; Di Sarno and Manfredi 2010; Barbagallo et al. 2017a) or base isolation (Clemente and Buffarini 2010; TahamouliRoudsari et al. 2018; Barbagallo et al. 2017b). The solutions aiming at increasing the structural capacity are invasive and generally expensive. The interventions that reduce the seismic demand could be advantageous, being less invasive and reducing installation time. In this field, friction connections (FCs) could be considered possible candidates for increasing the structural dissipation capacity (Khoo et al. 2015; Borzouie et al. 2016). Still, these devices are not common due to difficulties in their practical installation and the uncertainty of the RC building's coupled response. So far, full-scale experimental tests on the effect of asymmetric friction connections (AFCs) on RC frames are lacking (Rad et al. 2019; Khoo et al. 2013). However, many scholars started investigating the possibility of using timber as a strengthening solution for existing buildings, particularly cross-laminated timber (CLT) panels (Björnfot et al. 2017). In RC buildings with masonry infill, CLT panels can be used in addition or as substitution (Sustersic and Dujic 2013; Stazi et al. 2019) of existing masonry infill. The main issue related to these interventions is implementing an appropriate connection system between the CLT panel and the existing structure. The system

[1]Ph.D. Student, Dept. of Civil, Environmental and Mechanical Engineering, Univ. of Trento, via Mesiano 77, Trento 38123, Italy (corresponding author). ORCID: https://orcid.org/0000-0002-1039-386X. Email: francesco.boggian@unitn.it

[2]Ph.D. Student, Dept. of Civil Engineering and Architecture, Univ. of Catania, Via S. Sofia 54, Catania 5123, Italy. Email: carola.tardo@unict.it

[3]Research Fellow, Dept. of Civil, Construction and Environmental Engineering, Università degli Studi dell'Aquila, via Giovanni Gronchi 18, L'Aquila 67100, Italy. ORCID: https://orcid.org/0000-0002-6190-0139. Email: angelo.aloisio1@univaq.it

[4]Associate Professor, Dept. of Civil Engineering and Architecture, Univ. of Catania, Via S. Sofia 54, Catania 5123, Italy. Email: edoardo .marino@unict.it

[5]Professor, Faculty for Science and Technology, Norwegian Univ. of Life Sciences, Drøbakveien 31, Ås 1430, Norway. Email: roberto.tomasi@nmbu.no
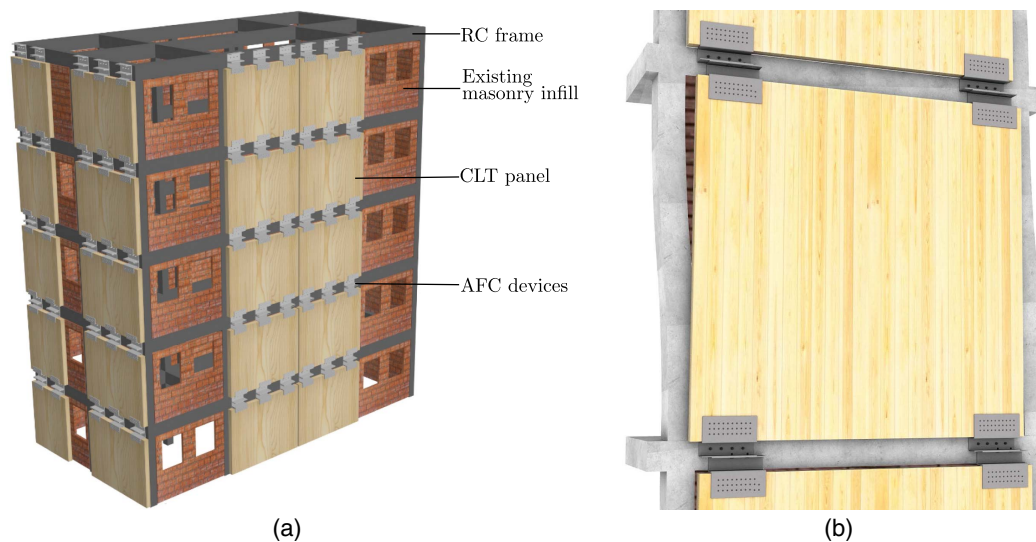
Fig. 1. (a) Components of the e-CLT retrofitting system; and (b) e-CLT panel subjected to seismic action.

proposed by the authors is called e-CLT (Fig. 1) and consists of installing a CLT panel from the outside of the building while leaving the masonry infills unchanged, without discomfort for the people living inside the building (Tardo et al. 2020). CLT panels have light weight (around 470 kg/m^3), thus not increasing too much the mass of existing buildings. Other advantages that make CLT attractive for retrofitting uses are the high level of prefabrication and the benefits of dry interventions, such as quick and easy installation, material recyclability, and reversibility of the retrofit intervention. The central innovation of the e-CLT retrofitting intervention stands in the connection system between CLT and the existing building: a friction connection. The FC is constituted by a couple of steel profiles, one connected to the existing beam and the other to the CLT panel, clamped together by preloaded bolts. One of the two profiles presents a slotted hole, which enables their mutual sliding. Single CLT panels are connected to the RC beams of the structure by at least two FC. The size of the CLT panels is related to that of the bays without openings where they are applied. In common RC framed buildings, the story height is generally equal to 3 m, while the width of each bay does not exceed 5–6 m. The e-CLT technology can be combined with nonstructural framed panels, which may be applied to the walls with openings and are equipped with high-performing windows that replace the existing ones. Both panels integrate insulation materials to improve the energy efficiency of the building and a finishing layer. The retrofit system also provides technological solutions to cover the FC devices after the panels installation and to ensure their inspection and maintenance (Margani et al. 2020).

This paper reports a testing campaign on the novel FC developed within the e-CLT retrofitting technology, but is also applicable to other types of structural panels or retrofit systems. The authors investigated the cyclic response of four different prototypes by focusing on their dissipative performance. The goal is to understand the prototypes' behavior for a mindful assessment of their potential for future developments. The main novelty of this paper lies in the development and testing of a new AFC for seismic retrofitting intervention coupled with CLT panels; both design choices regarding the shape and mechanical behavior of the system will be discussed. The investigation of the connection between FC and the CLT panel and between FC and the concrete beam is outside the scope of the current paper. The experimental activity was directed at isolating and studying the friction behavior of the FC, representing the innovative part of the system. The connections to the CLT panel and

to the concrete are known from the literature and standards. Their design will follow the capacity design rules with respect to the sliding force of the FC. The structure of the paper is as follows: after an overview of previous investigations on friction connections, tested specimens and setup are described; results are presented in graphical and tabulated form, along with a brief explanation of the data elaboration; a discussion completes the presentation of results, along with a possible modeling approach; and in the end conclusions are drawn.

Friction Connections

Several researchers investigated the performance of friction connections in their basic form, usually divided into two classes: symmetric friction connections (SFCs) and AFCs (Latour et al. 2019; Loo et al. 2014c). Symmetric friction connections present one central plate with an elongated hole and two lateral plates with round holes. In this connection, the central plate slides while the two lateral plates are restrained, determining symmetric loading conditions. In asymmetric friction connections, one plate is restrained while the other slides. This configuration determines asymmetric loading condition. A third plate with round holes may be used to close the connection as a cap plate. Additionally, shim layers made from various materials may be used between the three plates to increase the stability of the friction behavior. An example of the tested specimen, which is classified as AFC, is shown in Fig. 2.

Loo et al. (2012) initially used a numerical study to investigate the possibility of using SFC instead of hold-down for restraining timber shear walls against uplift, cap the force transmitted to the wall, and reduce inelastic damage. Consequently, Loo et al. (2014a, b) presented two experimental campaigns: the first on single SFCs and the second on full-scale timber walls. In Loo et al. (2014a) the focus was on the single connectors, with different materials tested as shim layers, such as brake lining and different alloys. An innovative connection without shim layers was also tested, where the central slotted element was made directly with the high-hardness alloy. They found that high-hardness alloys offered the best sliding performances, like Bisalloy 400, while steel versus steel sliding presented a more erratic behavior. In Loo et al. (2014b) the concept of SFC was applied to a full-scale timber wall, where the friction connections replaced the hold-downs. The results
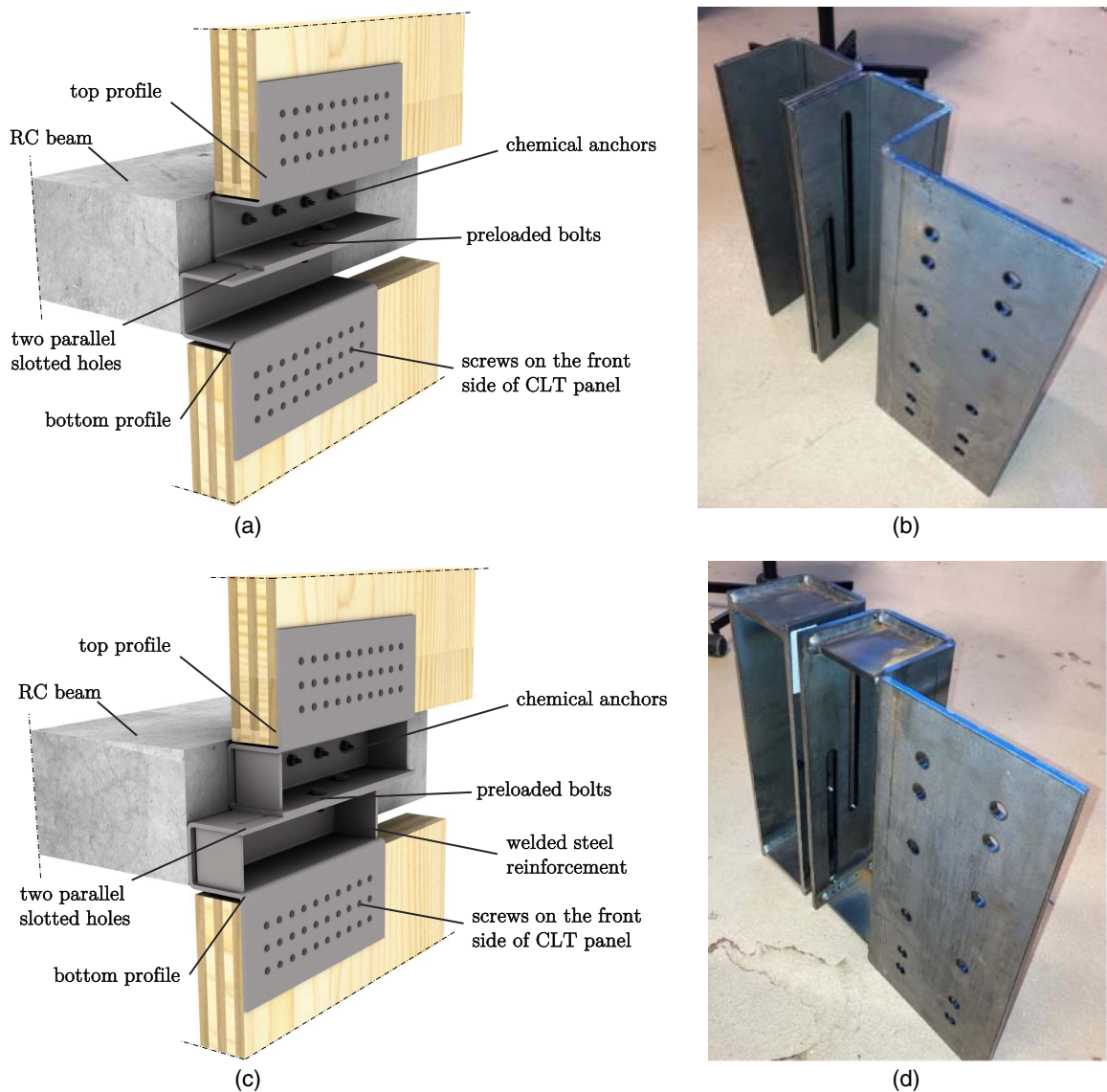
Fig. 2. (a) STD prototype; (b) STD specimen; (c) STD-R prototype; and (d) STD-R specimen.

showed that these devices determined a global elastoplastic response of the entire wall under cycling loading. Loo et al. (2016) further extended the concept by modeling CLT walls and multistory buildings and by proposing a displacement-based design method. Loo et al. (2017) tested SFC by adopting different methods of surface preparation of the sliding interface. Surfaces cleaned from loose rust and mill scale yielded the best hysteresis curves in terms of stability. Fitzgerald et al. (2021) studied an SFC with self-tapping screws for CLT, which was then also used for a full-scale campaign in Fitzgerald et al. (2020). Chanchi Golondrino et al. (2020) investigated the performance of SFCs in steel buildings. Golondrino et al. (2012a, b) presented two experimental campaigns on AFCs. The first (Golondrino et al. 2012a) aimed at understanding the behavior of the AFC when using different materials as shim layers. Materials with high hardness led to extremely stable loops, low-hardness materials determined moderately stable loops, while an erratic behavior was observed with medium-hardness materials (hardness values similar to steel plates). The second (Golondrino et al. 2012b) established a dependence between stability and shape of the loop and the clamping force level. Golondrino et al. (2016, 2020) presented an experimental campaign on AFC focused on the

bolt length effects. They found that increasing the bolt length determined a decrease in AFC strength and a more pronounced preload loss; conversely, the effective friction coefficient and its variability tended to decrease. Chanchí Golondrino et al. (2018) tested brake pads as shim material for AFC. Rodgers et al. (2018) studied the dynamic effects on AFC for applications in steel structures, which further led to the design proposals in Chanchi Golondrino et al. (2019).

Friction connections were selected as appropriate for the e-CLT seismic retrofitting intervention due to their highly efficient energy-dissipation mechanism, which contributes to reduce interstory drift damage to the existing building. The damage-free energy dissipation mechanism also ensures the durability of its structural efficiency even after seismic events. This feature avoids the need for the removal and replacement of the FC, which in turn would involve the removal of the attached CLT panel. After a seismic event, it is sufficient to check and eventually replace the bolts and the shim layers. Another important feature, different from viscoelastic devices, is that these connections present stable hysteresis loops that are not dependent on the speed (Jaisee et al. 2021).
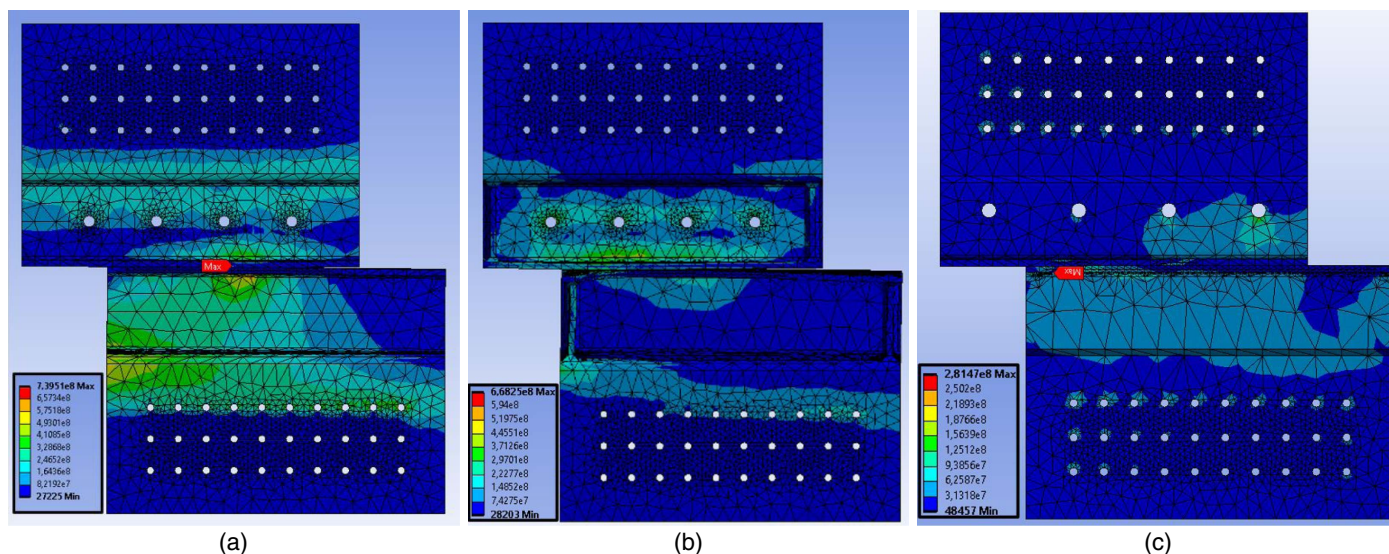
Fig. 3. FEM models from Tardo et al. (2020), showing equivalent von Mises stress (N/m^2) for a 30-kN sliding force: (a) STD design; (b) STD-R design; and (c) ALT design. (Images generated using Ansys, version 19.2.)

Materials and Methods

Specimen

The prototypes have four different geometries, all fabricated from 8-mm cold-bent S235 steel plates. The first is labeled STD, the standard design in Fig. 2(a), with an overall 450-mm width, 325-mm height, and 105-mm depth, which matches a 100-mm-thick CLT panel. Detailed dimensions are presented in the Appendix. The prototype consists of a couple of plates with different holes. The top profile has holes for the connections with the RC beam and round holes on the interface surface with the bottom profile. The bottom profile has two slotted holes, which guarantee the sliding between the two profiles. Each hole hosts a preloaded 10.9 Class M14 bolt. The clearance of movement is 100 mm in each direction, plus some tolerance. Both profiles present holes in the outer plates for screwed connections with the CLT panels. The STD is the initial design of the FC that worked as a base configuration. This configuration was conceived for the potential advantages in terms of industrial and technological efficiency also. On an industrial scale, the innovative design enables an easy and efficient manufacturing process because the profiles are produced by cutting, drilling, and press bending of steel sheets. These manufacturing processes are ordinary and commonly performed by workshops specialized in metal processing. Furthermore, the device allows for a fast and easy installation of the e-CLT system by means of mobile lifting equipment, thus avoiding the costs and time needed for the scaffolding setup. The inspection and maintenance interventions (e.g., preloading the friction bolts that may have loosened after a seismic event) are also facilitated by the front mounting and by adopting a proper cladding solution that covers the FC devices after the installation of the CLT panels. Even the swift removal and replacement of the dampers is possible because the steel profiles are connected to the external side of CLT panels.

Other three different designs were obtained by modifying the STD in order to improve the mechanical behavior and the possible weaknesses evidenced in finite-element modeling (FEM) (Tardo et al. 2020). The FEM analysis carried out in Ansys by Tardo et al. (2020) on the STD design highlighted significant stress concentrations and deformations around the bend of the bottom profile [Fig. 3(a)], which is the profile that is free to slide. Therefore, three

different prototype designs were derived from the STD, mainly by changing the following features: the number and position of the slotted holes, the out-of-plane eccentricity between friction connection and bottom profile (Fig. 4), and the number of bends of the bottom profile. Table 1 lists the names and features of all the designs. The prototype STD-R was built to add strength to the STD in the boxlike area, so two welded plates were added as reinforcements [Fig. 2(c)]. The two plates guarantee the same installation of the STD, without any grooves required in the CLT. The FEM analysis showed a partial improvement to the STD, even if the point of weakness remained in the area of the outer bend of the bottom profile, as seen from Fig. 3(b). The prototype STD-1H had the same geometry as the STD with one significant difference: there was a single and centered slotted hole with both preloaded bolts sliding inside [Fig. 5(a)]. This design originated from the simpler production process, faster mounting phase, and a more uniform force distribution between the two aligned bolts. The FEM investigations presented in Tardo et al. (2020) evidenced significant deformability of all the previous prototypes with STD shape due to (1) the eccentricity between the points of application of the slip force and the
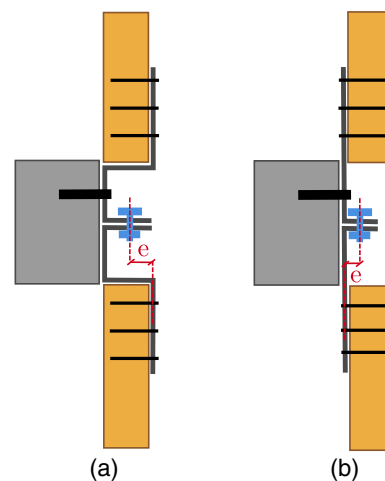

Fig. 4. Out-of-plane eccentricity of the system: (a) STD design; and (b) ALT design.

Table 1. Nomenclature and parameters of the prototypes

Prototype	Description	e (mm)	Slotted hole	n_{bend}
STD	Standard	46.1	Double	3
STD-R	Standard with reinforcements	46.1	Double	3
STD-1H	Standard with one elongated hole	46.1	Single	3
ALT	Alternative	32.8	Single	1

reaction force transmitted by the CLT panel, and (2) the multiple bends that characterize their geometry. Hence, in order to improve the expected performance, the authors developed the ALT prototype. The ALT design presents a shape different from that of the STD design, as shown in Fig. 5(c). In addition, the connection to the CLT panel was moved to the back, thus making both the profiles L-shaped elements. In this way, only one bend was necessary, and also the out-of-plane eccentricity could be slightly reduced. Furthermore, only one slotted hole was used for the bolts sliding, like the STD-1H prototype. As a result, the FEM analysis showed lower values of stresses and deformations if compared to the other designs, as seen from Fig. 3(c). However, the downside of this design is a more difficult mounting and maintenance procedure.

The connection to the CLT panel is on the backside, adjacent to the existing masonry.

The specimens used for the experimental campaign are shown in Figs. 4(b and d) and 5(b and d). They present some modifications with respect to the prototypes, mainly related to the choice of test setup and goal of the campaign, the study of the sole friction connection. Each specimen was composed by two profiles. One profile was shaped as the bottom profile of the corresponding prototype, and presented 12 holes to be fixed by means of bolts to a steel column, which simulated the CLT panel. The other profile was C-shaped and simulated the top profile fixed to the RC beam, which was replicated by a steel element. The displacement protocol of the press simulated the horizontal displacement of the RC beam of the existing building. The authors assumed the possible application of the e-CLT technology in RC buildings characterized by a prevalent shear-type behavior. Therefore, the floors mainly exhibited a horizontal displacement, and no uplift was allowed to the CLT panel.

Setup and Load Protocol

The authors devised the setup to test the four different specimens with minor adjustments, despite the STD and the ALT specimens
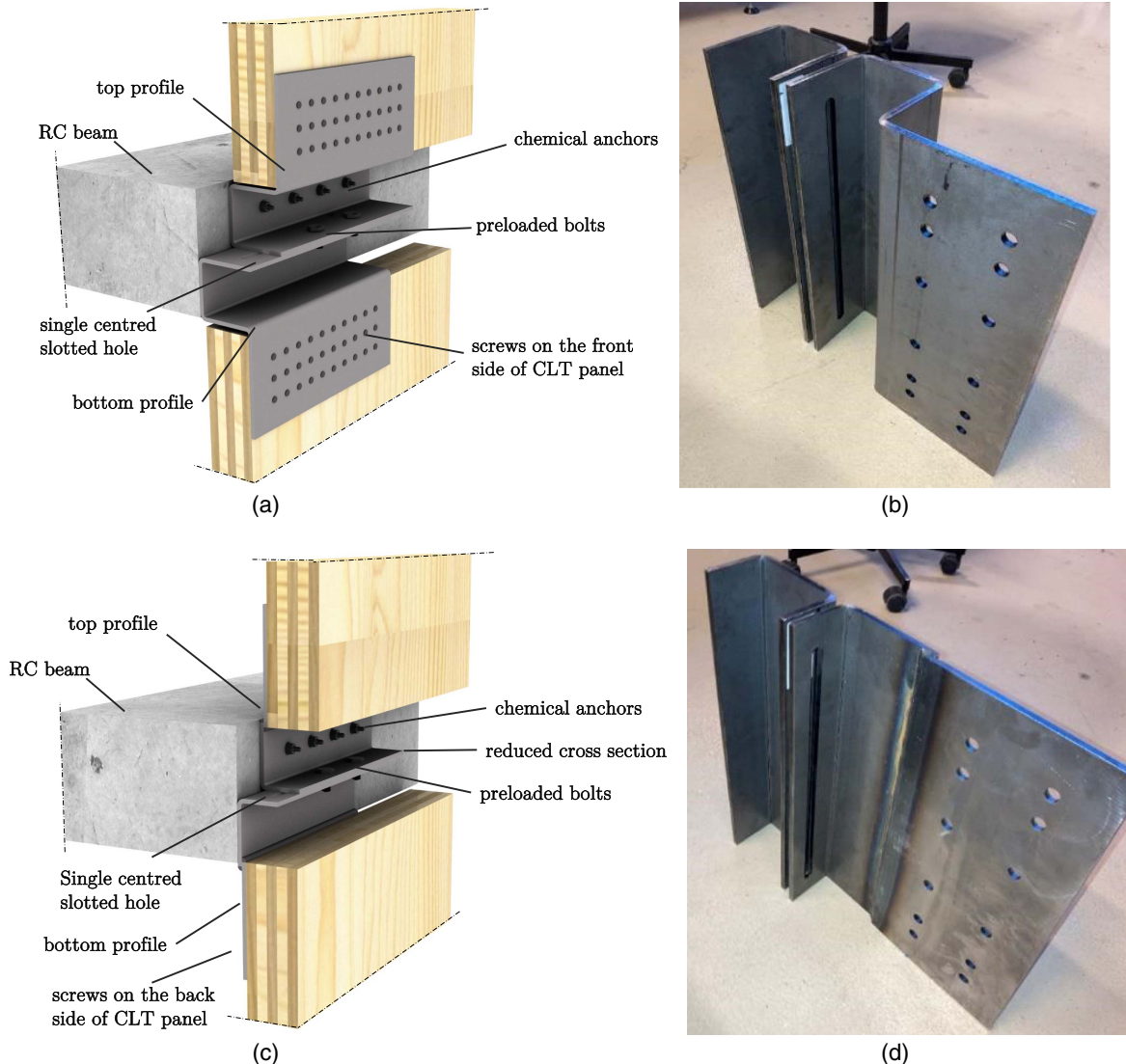

Fig. 5. (a) STD-1H prototype; (b) STD-1H specimen; (c) ALT prototype; and (d) ALT specimen.
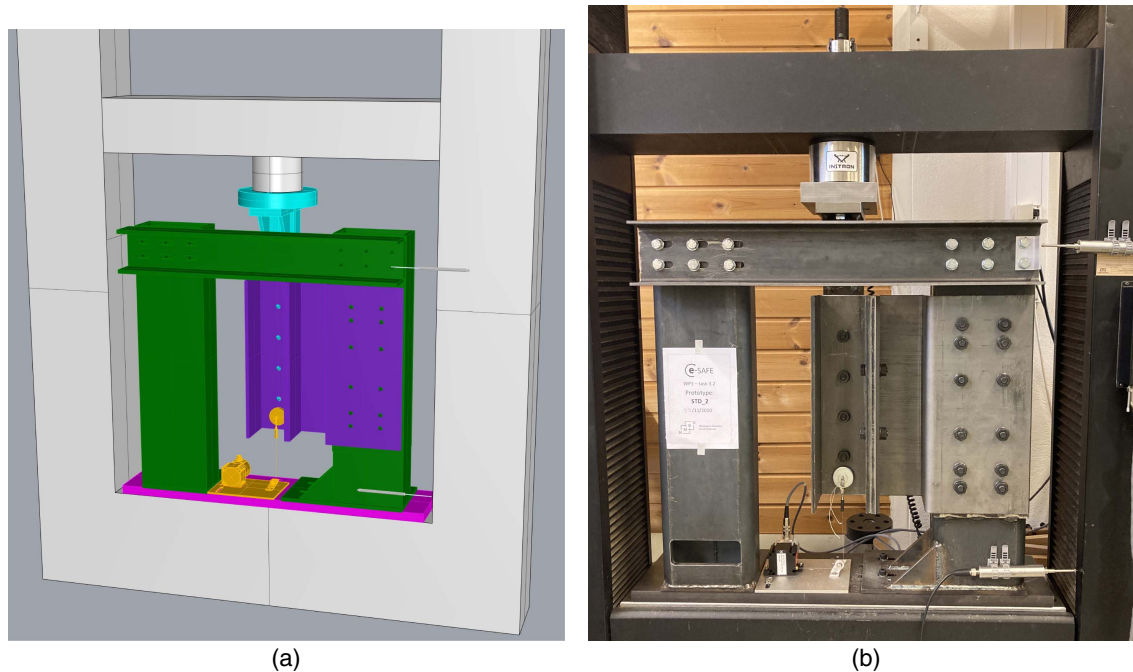
Fig. 6. (a) Three-dimensional model of the setup; and (b) setup.

having different geometry. The setup was conceived to reproduce a loading condition that applies a sliding movement to the FC in order to isolate and study the friction behavior. The setup consists of a rigid steel frame embedded in a universal Instron electromechanical testing machine, as seen in Figs. 6 and 7. The two columns present a rectangular hollow steel section, 12.5-mm thick and 100×120 mm dimension. The bottom profile of each specimen is fixed on the right column from the outside, using 12 prescrewed bolts. A T-shaped element ensures the load transfer to the specimen: its base stands below the load cell, while the C-shaped top profile is connected to its wing, which simulates the RC beam movement.
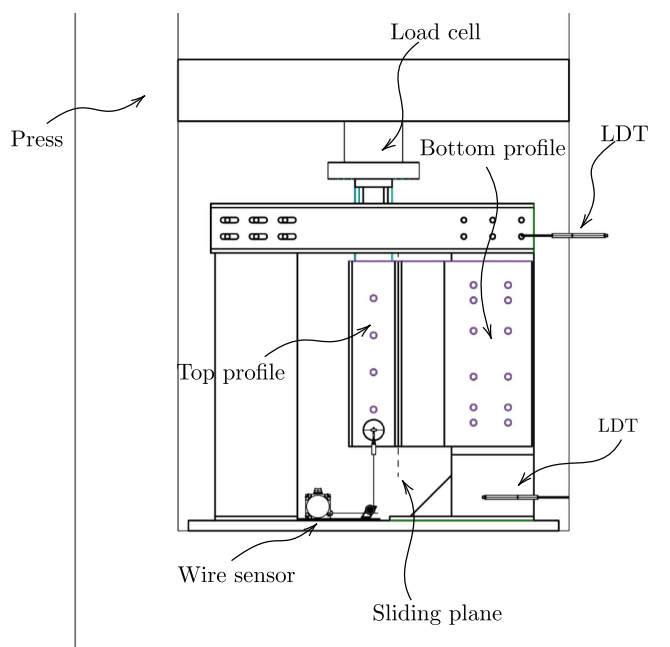

Fig. 7. Setup elements and measuring acquisition system.

The column-base connection of the right column, the left beam-to-column connection, and the connection between the T-element and press plate are realized by means of slotted holes. The clearance of the slotted holes was designed to accommodate manufacturing tolerance of the specimens.

With a 100- and 50-kN capacity in monotonic and cyclic testing, respectively, the press load cell measures the force. Two sensors measure the top profile displacement: the sensor embedded in the press, which drives the displacement-controlled test, and an external wire sensor attached to the bottom profile with a magnet. LVDTs also acquired two displacement measures on the right column, by its base and top, to detect undesired sliding or rotations for assessing the adequacy of the setup stiffness. A scheme of the measuring setup is provided in Fig. 7.

The displacement-controlled loading protocol originates from the approach in ISO 16670 (ISO 2003) and EN 15129 (CEN 2018a): both standards suggest a cyclic protocol with incremental steps of percentages of the ultimate displacement. For the friction connection, the maximum sliding clearance is given by the length of the elongated holes: the ultimate displacement for the tests descends from a geometric property and is set equal to the hole sliding length of 100 mm. The choice of this sliding length value derives from the assumption that typical RC frame structures reach failure for an interstory drift close to 3% of the story height. Common buildings to be retrofitted with the e-CLT system have a story height of approximately 3 m. Therefore, the sliding length was chosen to be 100 mm, having some tolerance. The load protocols are presented in Table 2 and Fig. 8.
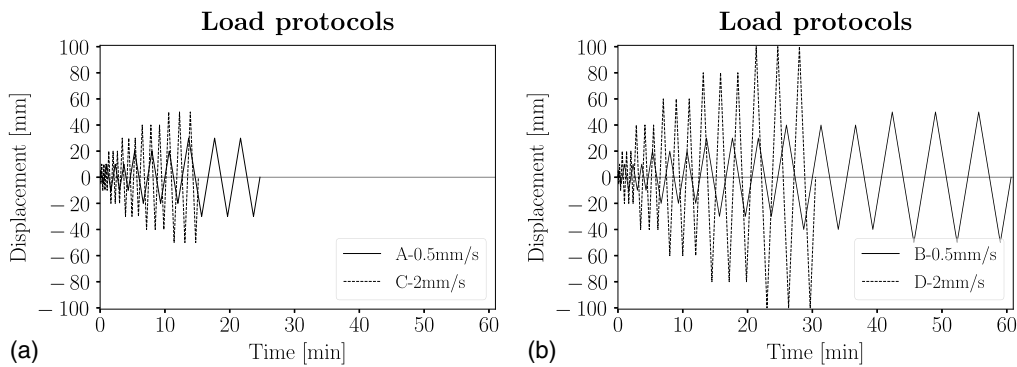
Test Overview

Table 2 lists the tests carried out in this campaign. The investigation consisted of two main parts. In the first instance, for Tests STD.1 to STD.4, the authors did not use shim layers or cap plates to examine the steel-to-steel erratic response and determine the consequences of the cap plate absence. In the second part of the tests, the authors
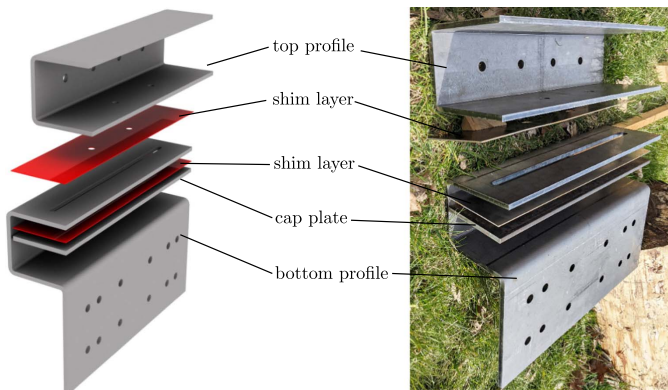
Table 2. Test overview

Test	Specimen	Protocol	Speed (mm/s)	Shim	Preload (kN)
STD.1	STD_0	Monotonic	4.0	—	80.5
STD.2	STD_1	Cyclic A	0.5	—	24.1
STD.3	STD_1	Cyclic B	0.5	—	24.1
STD.4	STD_1	Cyclic B	0.5	—	24.1
STD.5	STD_2	Cyclic B	0.5	Aluminum	24.1
STD-R.1	STD-R_1	Cyclic B	0.5	Aluminum	24.1
STD-1H.1	STD-1H_1	Cyclic B	0.5	Aluminum	24.1
STD-1H.2	STD-1H_1	Cyclic B	0.5	Aluminum	45.3
ALT.1	ALT_1	Cyclic B	0.5	Aluminum	24.1
ALT.2	ALT_1	Cyclic B	0.5	Aluminum	36.0
ALT.3	ALT_1	Cyclic C	2.0	Aluminum	36.0
ALT.4	ALT_1	Cyclic D	2.0	Aluminum	36.0

Note: Cyclic A: 1×5 mm + 3×10–20–30 mm, speed 0.5 mm/s; Cyclic B: 1×5 mm + 3×10–20–30–40–50 mm, speed 0.5 mm/s; Cyclic C: 1×5 mm + 3×10–20–30–40–50 mm, speed 2 mm/s; Cyclic D: 1×5–10 mm + 3×20–40–60–80–100 mm, speed 2 mm/s.

Fig. 8. Load protocols: (a) Cyclic A = 0.5 mm/s, Cyclic C = 2 mm/s; and (b) Cyclic B = 0.5 mm/s, Cyclic D = 2 mm/s.

included an 8-mm cap plate and 2-mm aluminum shim layers, as shown in Fig. 9, thus reproducing an AFC. The first test was monotonic, with a preload force of the bolts that clamp together the two profiles of the specimen equal to 70% of the bolt ultimate tensile strength, while the others were cyclic with a lower preload force. The lower preload force depended on the testing machine limitations in cyclic testing. Therefore, the authors preloaded the bolts to achieve an approximate 30-kN slip force. The loading condition is not symmetric and the specimen presents a complex shape. Therefore, the authors expect the occurrence of a certain deformation level; see Tardo et al. (2020) and Hatletveit (2020) for FEM analyses of the specimen. The testing procedure was the following: the bottom profile was mounted on the right column and the top profile was mounted on the T-element. Each component was then

Fig. 9. Parts of a specimen.

aligned before inserting and preloading the two bolts that clamp the two profiles together and form the friction connection. A torque wrench was used to give the bolts the preload force, according to the torque method prescriptions of EN 1090 (CEN 2018b) and the bolt producer instructions (SBE-Varvit 2021).

Results

This section illustrates the results of the testing campaign. Figs. 10–12 show the results in graphical form for all the specimens. For each specimen the first graph represents the force displacement loops, which provides insight on the overall behavior of the friction connection. The second graph visualizes the measured force plotted against time for an enhanced readability of the stability of the force throughout the experiments. The third graph presents the dissipated energy during testing, which is a useful parameter for the definition of the slip force because it is an increasing function. Table 3 summarizes the results by reporting significant values defined in the following paragraphs.

The definition of the slip force F_{slip} from the experimental data is neither straightforward nor unique. The author decided to use the same approach used by Loo et al. (2014a), which adopts a definition related to the dissipated energy E

$$E = \sum_{i=0}^{n} E_i = \sum_{i=0}^{n} \left| \frac{F_{i+1} + F_i}{2} \cdot (\delta_{i+1} - \delta_i) \right| \quad (1)$$

where E_i = energy at the ith time step; and F_i and δ_i = force and displacement at the same time step, respectively. The dissipated energy presents a strictly increasing trend, and is therefore a useful
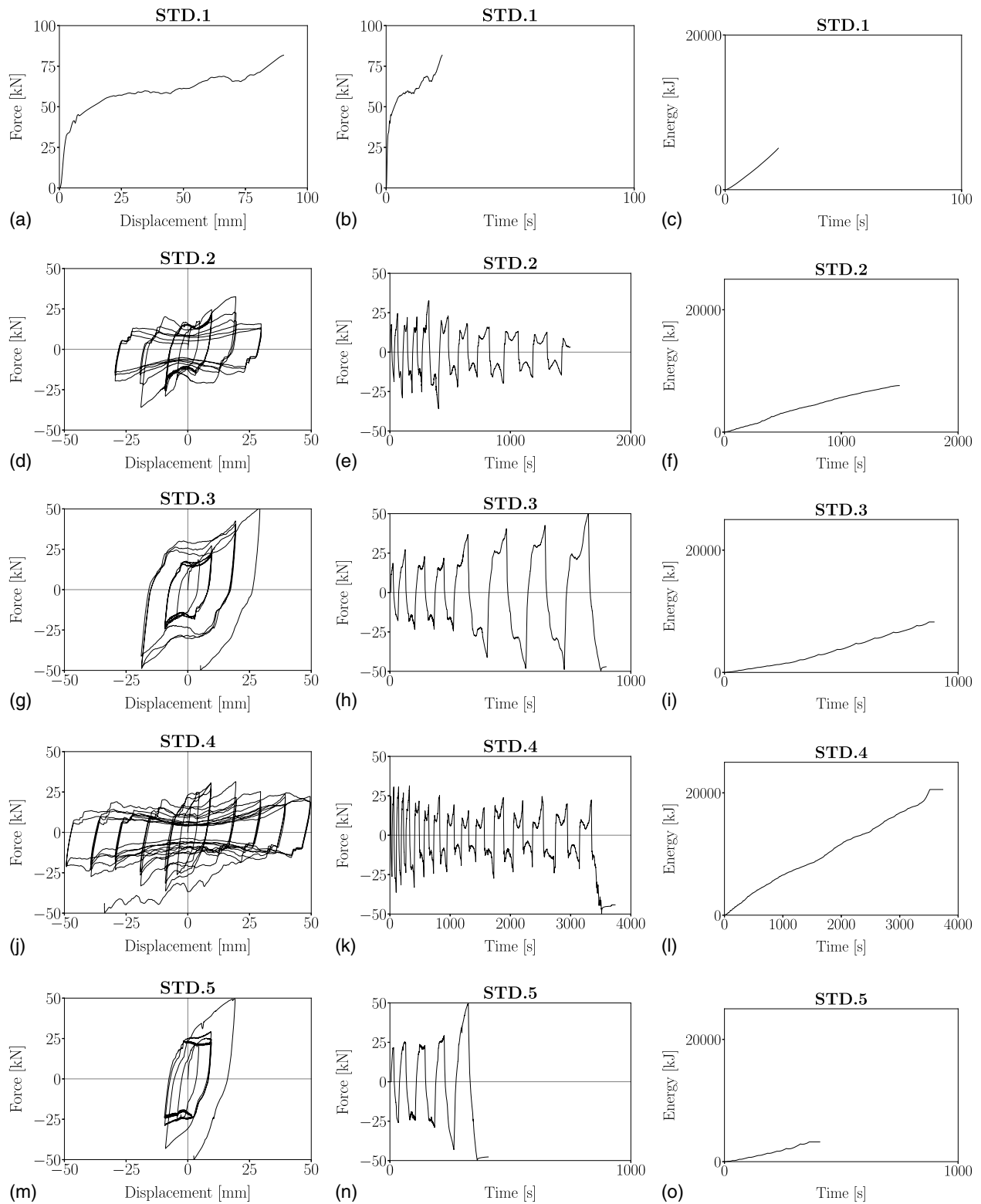
Fig. 10. Test results of STD specimens.

unambiguous parameter for the calculations, as opposed to the force value. The cumulative distance of travel D is the sum of the displacement time steps

$$D = \sum_{i=0}^{n} |\delta_{i+1} - \delta_i| \qquad (2)$$

The slip force is defined as the work per unit of length

$$F_{slip} = \frac{E}{D} \qquad (3)$$

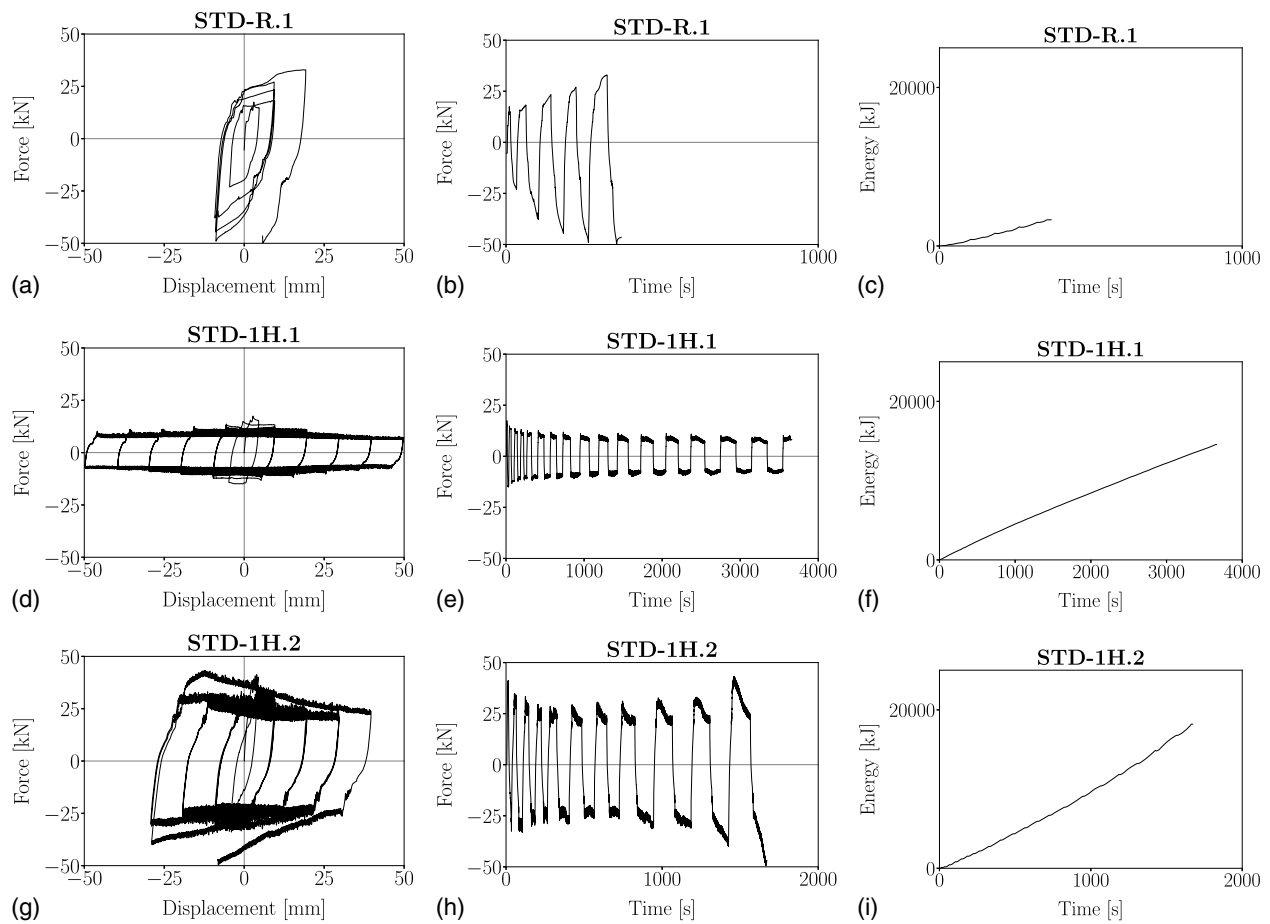The standard deviation is calculated with reference to the F_{slip} value

Fig. 11. Cyclic test results of STD-R and STD-1H specimens.

$$F_{sd} = \sqrt{\frac{\sum_{i=0}^{n} |F_i - F_{slip}|^2}{n-1}} \qquad (4)$$

The coefficient of variation (COV) and the stability parameter λ are calculated as follows:

$$\text{COV} = \frac{F_{sd}}{F_{slip}} \qquad \lambda = \frac{1}{\text{COV}} \qquad (5)$$

These two values express the loop stability and the sliding behavior nature: a low COV, and thus a high λ value, corresponds to stable performance, resembling the ideal rectangular shape. The experimental friction coefficient μ is calculated as follows:

$$\mu = \frac{F_{slip}}{n_s n_b F_P} \qquad (6)$$

where F_{slip} = slip force calculated in Eq. (3); n_s = number of shear surfaces; n_b = number of preloaded bolts; and F_P = preload force from Table 2.

Fig. 13 attempts to capture an essential aspect of the tests on friction connections: the definition of F_{slip} is substantially dependent on the loading path, while its value is not constant during the test. The authors present the final values in Table 3 related to each test. They also plot their time dependency in Fig. 13. The x-axis represents the displacement step (see Table 2 for the list of the displacement steps of the various load protocols), while, on the y-axis, the circles represent the slip force calculated from the beginning of the test up to a specific displacement step. Fig. 13 manifests two sorts of scatter:

the horizontal variation, relative to changes in slip force between successive displacement steps, and the vertical variation. The latter derives from the repetition of three cycles at the same displacement step: an appreciable vertical distance between the three circles representing F_{slip} indicates a considerable variation of force during the repetitions of the same displacement step. In Fig. 13, the authors also report the friction coefficients, which follow the same trend of the slip force.

Discussion

The first test, the monotonic STD.1, evidenced the weak point of the STD design from the very beginning. The outward bend of the bottom profile suffered from big deformations, which determined the test to stop. The FEM analysis in Tardo et al. (2020) also confirms the presence of strong stress concentrations in that area; additional information is available in Hatletveit (2020) and Marthinsen (2020). The load–displacement curve shows that the slip force was approximately 60 kN [Fig. 10(a)]. However, when the deformation of the bottom profile increased, the bolts started pressing against the side of the holes, thus increasing the resisting force. The increased resisting force did not depend on friction solely, but it was a combination of friction and bolts-holes plasticization. The deformations originated from the eccentricity between the applied force and the bend of the bottom profile: the upper part deformed outward while the lower part deformed inward, as seen in Fig. 14(a). Another significant deformation was a relative twisting between the two sliding surfaces, which made the previous
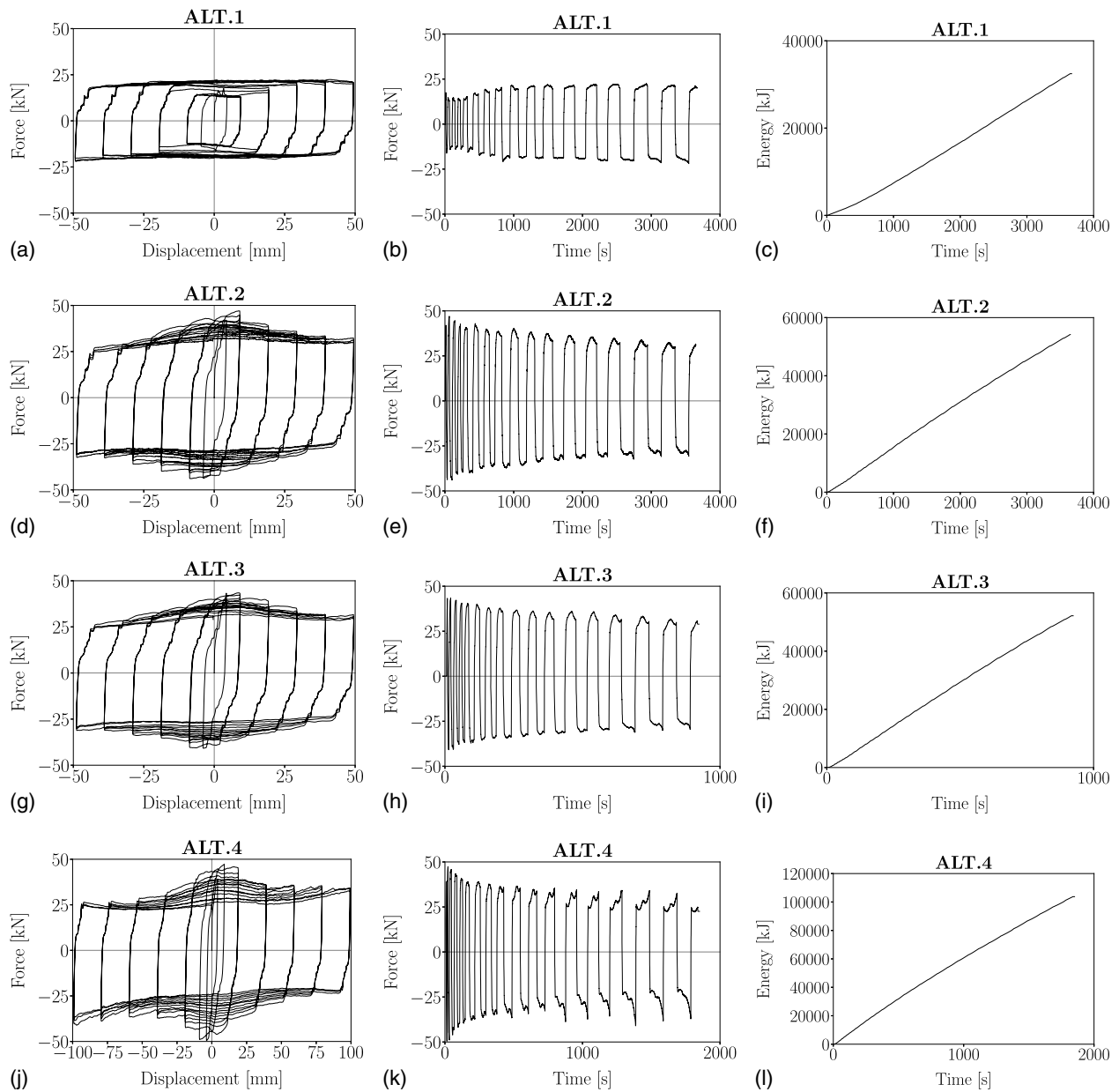
Fig. 12. Cyclic test results of ALT specimens.

Table 3. Results of cyclic tests

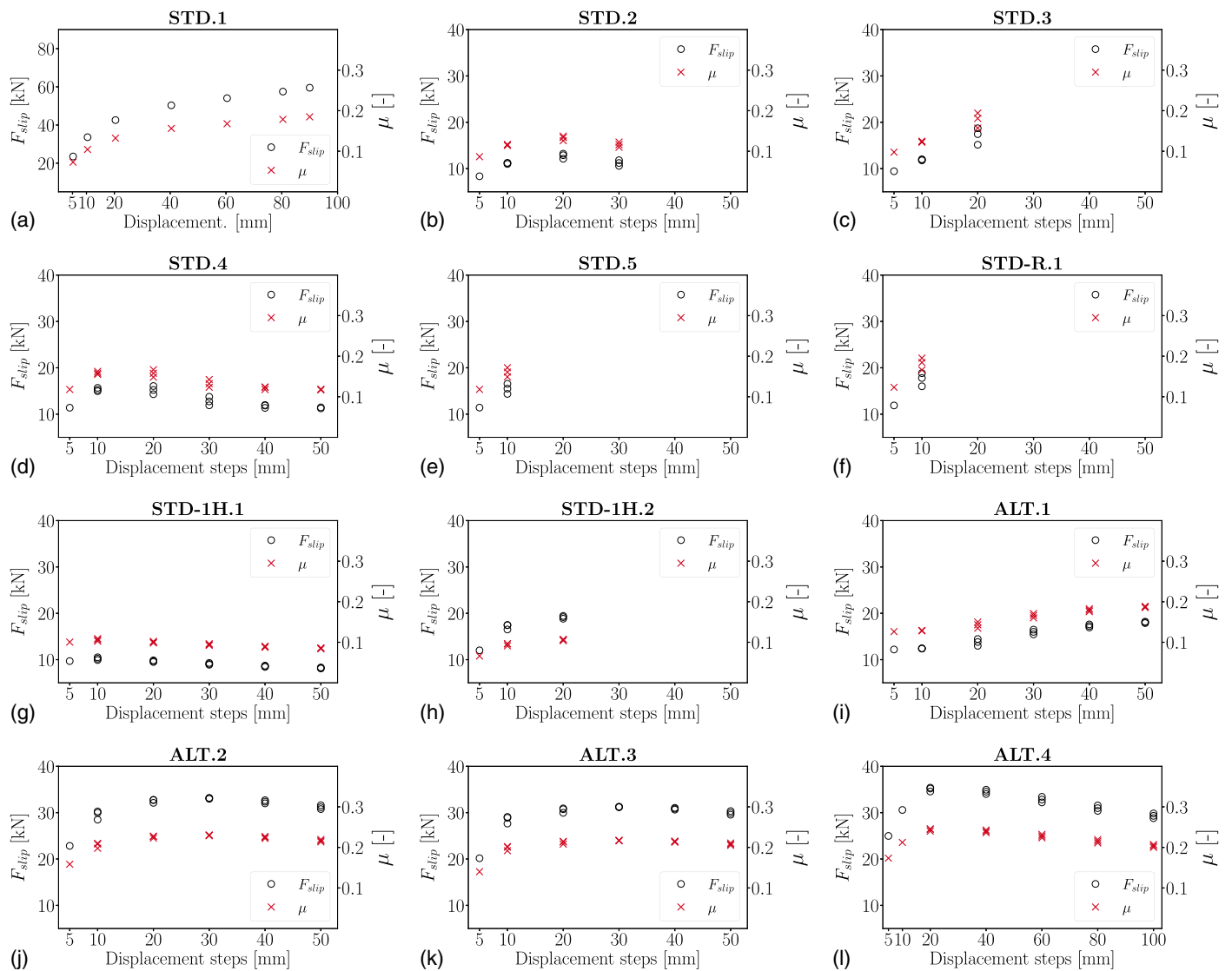| Test	F_{slip} (kN)	F_{sd} (kN)	COV	λ	μ	Preload loss
STD.1	59.94	12.11	0.20	4.95	0.19	Yes
STD.2	10.61	5.62	0.53	1.89	0.11	Yes
STD.3	19.99	12.02	0.60	1.66	0.21	No
STD.4	12.00	10.59	0.88	1.13	0.12	Yes
STD.5	19.51	14.78	0.76	1.32	0.20	No
STD-R.1	20.49	12.79	0.62	1.60	0.21	No
STD-1H.1	8.10	1.44	0.18	5.62	0.08	Yes
STD-1H.2	22.74	8.53	0.38	2.67	0.13	No
ALT.1	18.20	3.62	0.20	5.02	0.19	Yes
ALT.2	30.79	7.51	0.24	4.10	0.21	Yes
ALT.3	29.57	7.27	0.25	4.07	0.21	Yes
ALT.4	28.79	6.80	0.24	4.23	0.20	Yes

Fig. 13. Variation of slip force and friction coefficient during testing.

effect even worse and was caused by the eccentricity between the two preloaded bolts, also marked in Fig. 14(b). Testing of the STD design specimen, despite some expected issues, was important to have a base for comparison with further improvements. The goal was to understand if, with some improvements and small modifications of the STD design, it was possible to achieve satisfactory mechanical behavior with a design the offers the frontal mounting possibility.

In the STD.2, STD.3, and STD.4 tests, the preload force was lowered to 30% of the previous values and the speed was also reduced to 0.5 mm/s in order to obtain a lower slip force and minor deformations of the specimen. The curves of these tests, depicted in Figs. 10(d, g, and j) and compared in Fig. 15, exhibit an extremely erratic shape, with unpredictable behavior: Tests STD.2 and STD.4 present similar shapes and level of forces, while STD.3 reached higher forces rapidly, thus causing the stopping of the test before the completion of the whole protocol. Both Tests STD.2 and STD.4 exhibited preload losses in the bolts at the end of the test, but STD.3 did not. This occurrence may be the motivation for such prominent differences in behavior. In both STD.2 and STD.4, the hysteresis loops are remarkably similar, presenting a sudden drop in force after the initial peaks, possibly indicating the instant of preload

loss. Twisting deformations were more pronounced throughout the whole duration of Test STD.3, which was the one that retained the preload until the end of the test, if compared to STD.2 and STD.4. The STD.2 and STD.4 tests also presented twisting deformations, mostly during the initial part of the test. In all these experiments, significant deformations were always present in the outer bend of the bottom profile. The authors also observed a notable scraping of steel between the washers and the sides of the holes.

Test STD.5 had two modifications: an 8-mm steel cap plate to limit steel scraping and two shim layers made with 2-mm-thick aluminum to obtain more stable loops. The authors maintained this AFC configuration throughout the rest of the campaign. Nevertheless, the performances of STD.5 were still poor [Fig. 10(m)]. As observed in the previous cases, STD.5 exhibited considerable deformations and consequent force spikes, which did not allow the completion of the loading protocol. The force continued increasing, with the absence of preload losses at the end of the test. Again, the resisting force did not depend on the sole friction, but it was a combination of friction and bolts pushing against the holes. The values of the slip forces and friction coefficients of the STD tests, reported in Fig. 13, are then rather approximate, because the tests did not exhibit a pure frictional behavior.
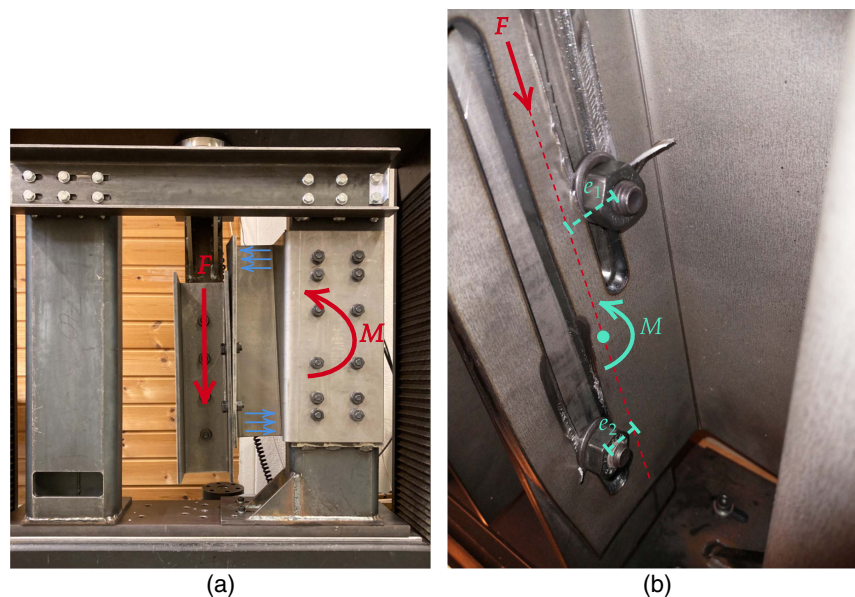
Fig. 14. Test STD.1: schemes illustrating the observed deformations.

Although the STD-R.1 specimen had additional reinforcements, the behavior was comparable to the STD.5 test [Fig. 11(a)]. The reinforcement in the boxlike part of the specimen contributed to isolate the weak spot evidenced during the FEM analyses even more: the outer bend of the bottom profile. Twisting was also present, and the large deformations and rapid force increase led the experiment to an early stop, as in the previous case.

STD-1H.1 showed an almost rectangular loop behavior, shown in Fig. 11(d). Twisting deformation was significantly reduced, indicating that a proper bolt arrangement in a single slotted centered hole effectively mitigated the detrimental phenomena identified for Specimens STD and STD-R. The lower force level also determined a lower bending deformation than in previous cases. The preload was lost at the end of the test. This aspect also emerges from observing the value of the slip force, which presents some initial peaks around 16–17 kN, later declining to $F_{slip} = 8.1$ kN, as shown in Table 3 and Fig. 13(g). In the same figure, it is possible to see that the friction coefficient value is unexpectedly small.
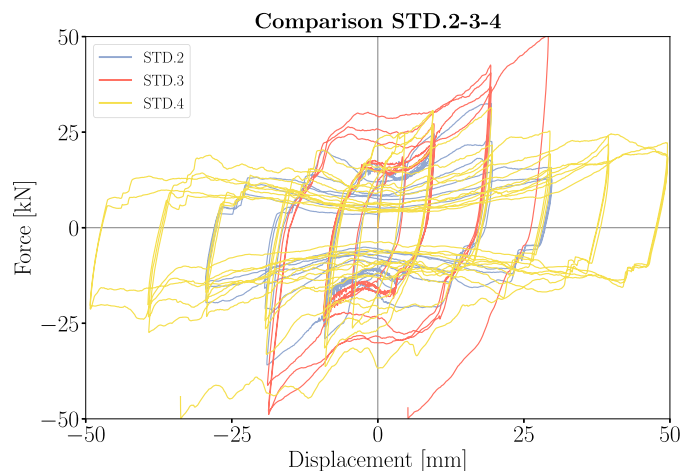
This value depends on the assumption of the initial preload force value used for calculation, which in reality decreased during the test. In Test STD-1H.2, the authors increased the preload to obtain a higher slip force. Still, higher deformations also occurred. Twisting was more evident than in the previous case, even if more limited than in the STD specimens. The bending deformations were quite noticeable during this test, possibly due to the absence of significant preload losses. This phenomenon suggests that higher stresses arose inside the bottom profile. The force rapidly increased to the 50-kN limit value of the testing machine during the early cycles; therefore, the test stopped before the completion of the entire Load Protocol C.

The ALT specimen showed promising results. The loops in Fig. 12(a) closely resemble a rectangular shape, and the force level agrees with analytical predictions. The friction coefficient is in accordance with scientific literature (Golondrino et al. 2012a), approximately equal to 0.2 for aluminum, as observed from Fig. 13(i). Both twisting and bending deformations were almost absent during this test, meaning that the reduced eccentricity and the single bend played a vital role in obtaining stable loops, confirming the initial FEM results of Tardo et al. (2020). The loop shape presents a corner chipping when the load is changing direction: this is common in asymmetrical friction connections (Loo et al. 2014a; Fitzgerald et al. 2021) and depends on dragging phenomena of the cap plate. The preload force was then increased in the remaining tests on the ALT design, with the goal of reaching a 30-kN slip force. The ALT.2 results, shown in Fig. 12(d), present a lightly less stable behavior. Still, the slip force and friction values agree with the expected ones, as confirmed by Fig. 13(j). One significant difference in shape concerning the previous test regards the first cycles. There were lower initial resisting forces in Test ALT.1, stabilizing at higher values close to the slip force. Conversely, there were more prominent peaks in the initial cycles of Test ALT.2, which then gradually declined and reached the stable force level. This aspect is also evident when comparing Figs. 13(i and j): while in the first case, it is possible to seize an increasing trend of the plotted F_{slip} development, in the second case, after the peak, the trend is decreasing. Test ALT.3 included a change of speed: from 0.5 to 2 mm/s. The results prove that the change in speed did not have any noticeable effect on the connection behavior, as highlighted by
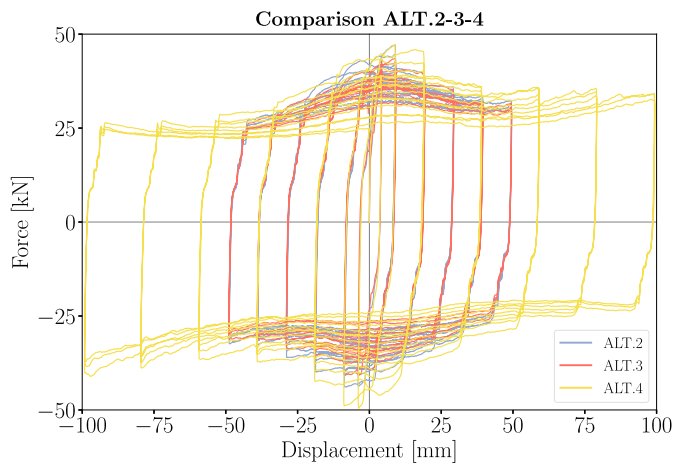

Fig. 15. Comparison of the results of Tests STD.2, STD.3, and STD.4.

Fig. 16. Comparison of the results of Tests ALT.2, ALT.3, and ALT.4.

where $F_{\mathrm{slip}}(\epsilon)$ = slip force; F_P = preload force; $\dot{d}$ = time derivative of the displacement; and ϵ = cumulated dissipated energy. The friction coefficient is defined as

$$\mu(\epsilon) = \mu_0(e^{-\xi\epsilon} + 1) \qquad (8)$$

where μ_0 and ξ = parameters estimated from the experimental data. As an example of application, Fig. 17 shows the superposition of experimental data and simulated model for the Test ALT.3; the parameters $\mu_0 = 0.33$ and $\xi = 0.00005$ were estimated from an ordinary least-squares optimization.

The proposed model accurately reproduces the experimental behavior, including the effect of decreasing slip force values for higher cycles. The energy dissipation is higher than the experimental value, and this is caused by the nonrectangular shape of the experimental loops due to the corner chipping effect of asymmetric friction connections. The simple proposed model, on the other hand, generates loops with perfect rectangular shape, thus leading to higher dissipated energy values. The authors neglect this phenomenon at this stage, given the limited impact on the dissipated energy.

the comparison in Fig. 16, thus confirming one positive feature of friction connections: being independent from the speed of loading. The specimen was also the same as in the previous test, indicating that the connection response does not suffer cumulative damages. Friction coefficient values again agree well with Golondrino et al. (2012a), who found a dynamic friction coefficient value of 0.18 for aluminum and a static value of 0.34. The present test provides a friction coefficient value of 0.21 (dynamic condition) and a value of 0.33 when referred to F_{peak} (static initial condition). ALT.4 was the last test, and in this case the displacement protocol reached the full 100-mm sliding capability of the slotted holes. The load–displacement graph shows that up to 50 mm, the behavior is the same as the previous tests, while for higher levels of displacements, there is a moderate loop instability. In these last three tests, slight twisting deformation was observed mainly at the change of direction of the load and not continuously as in the STD and STD-R design.

Friction Model

This section presents a possible approach for the simulation of the observed experimental behavior for inclusion in further nonlinear dynamic analysis. The performance of the AFC is mainly related to Coulomb friction. The function defining the friction force must take into account the observed force decrease with cycles

$$F_{\mathrm{slip}}(\epsilon) = \mu(\epsilon)F_P\mathrm{sign}(\dot{d}) \qquad (7)$$

Conclusion

This paper presents a testing campaign on a novel FC for seismic retrofitting of an existing RC frame building. The entire system, called e-CLT, is part of the European Horizon (2020) project e-SAFE. The seismic retrofitting originates from the installation of CLT panels attached to the outside of a building with innovative friction connections. The connections are asymmetrical friction connections, composed of a couple of cold-bent steel profiles. One steel profile is connected to the CLT panel, while the other is connected to the RC beam. The two profiles are held together by preloaded bolts, which can slide in slotted holes and dissipate energy via friction. This paper focuses on the experimental tests of the FCs for the estimation of their dissipative capacity. The authors carried out an experimental campaign on four different geometries: the standard (STD), two variations [one with reinforcements (STD-R) and one with a single elongated hole (STD-1H)], and an alternative with reduced eccentricity and lower number of bends (ALT). The main findings were that STD and STD-R suffer from major deformations due to bending and twisting, and the reason lies in two features: an intrinsic weakness of the outer bend of the bottom profile, because of the eccentricity, and the presence of two not aligned elongated holes. STD-1H and ALT showed promising results, indicating that the arrangement of a single elongated hole solved some of the deformation problems and that the reduced eccentricity and lower number of bends of ALT design was effective in isolating
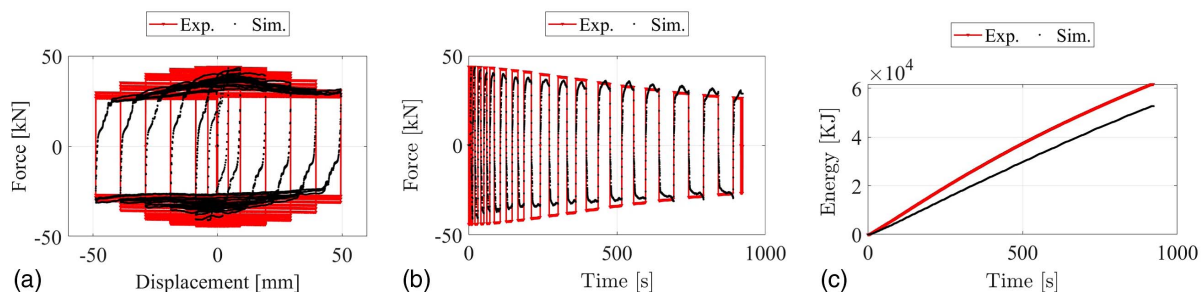

Fig. 17. Comparison of experimental data and exponential friction model: (a) force–displacement loop; (b) force–time function; and (c) cumulated dissipated energy–time function.

the friction behavior. The authors obtained acceptable results using aluminum for the shim layer, whose friction coefficient, nearly equal to 0.2, agrees with literature formulations. Aluminum as shim material provided stable hysteresis curves, while its absence caused an erratic response (e.g., steel-to-steel friction). ALT tests also confirmed the independence from loading speed of the friction connections. A possible modeling strategy was presented based on an exponential Coulomb friction model that reproduces

the observed experimental behavior. In general, the main conclusions are that
• The out of plane eccentricity, between the sliding force and the CLT restraint on the bottom profile, and the number of bends play the most important role: a limited depth of the connectors, aimed at reducing the eccentricity, and a single bend are effective in limiting unwanted deformations and isolating the friction behavior.
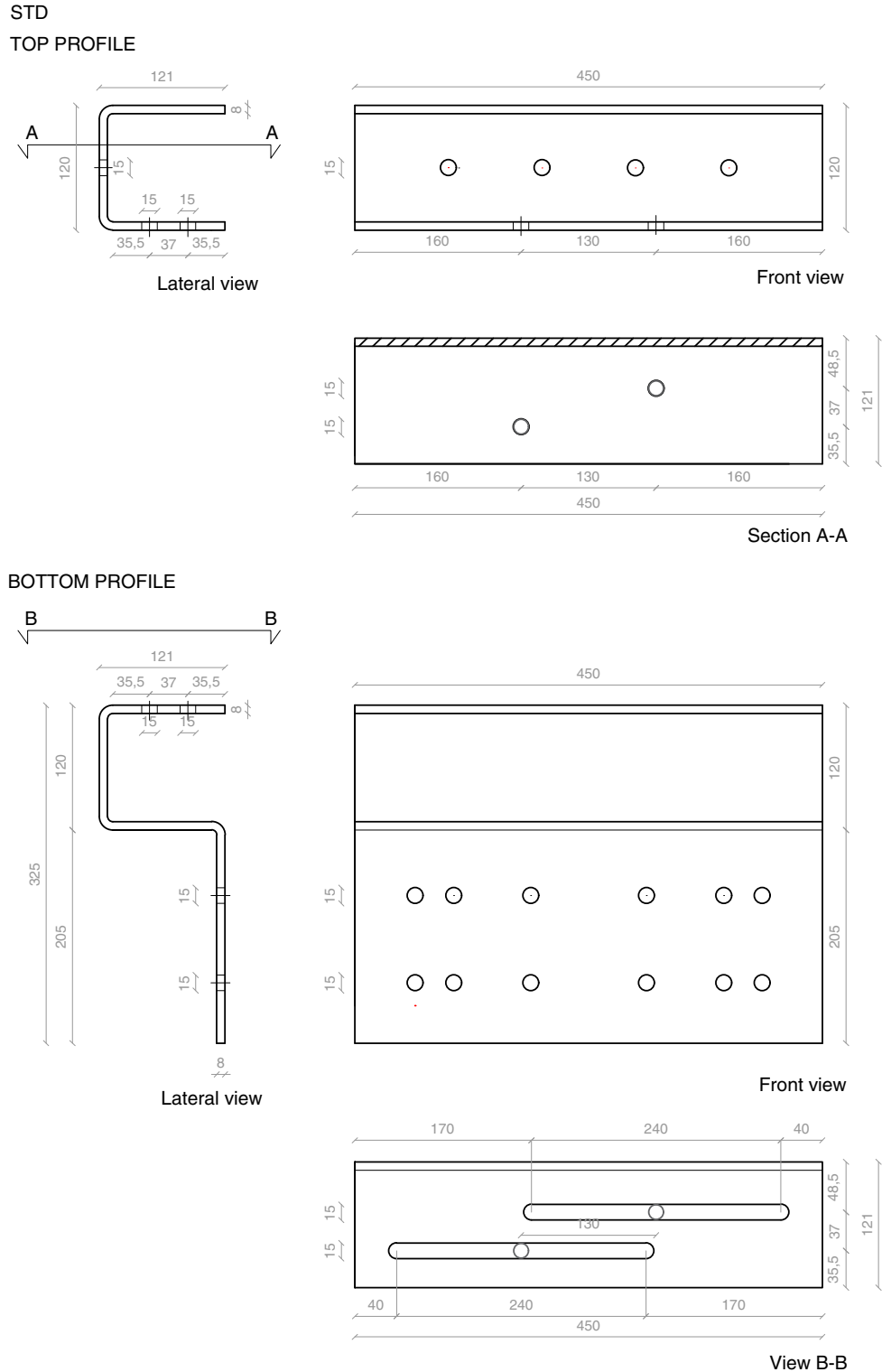

Fig. 18. STD specimen, measurements in millimeters.

- The arrangement of the bolts in two unaligned slotted holes is a cause of additional eccentricities during the sliding movement: a single slotted hole with both bolts aligned is preferable to limit twisting deformations.
- A cap plate and shim layers are necessary to obtain an acceptable loop stability: aluminum shims provided satisfactory frictional behavior with an estimated 0.2 friction coefficient.

- An exponential Coulomb model represent a satisfactory strategy to model the observed experimental results of the AFC.

The major limitation of the experimental campaign presented in this paper is the limited number of specimens tested and replications. However, these tests allowed studying the system at a small scale related to the friction connection, which was useful to investigate the potential of the system. The tests confirmed that the performance parameters of the system are related to the
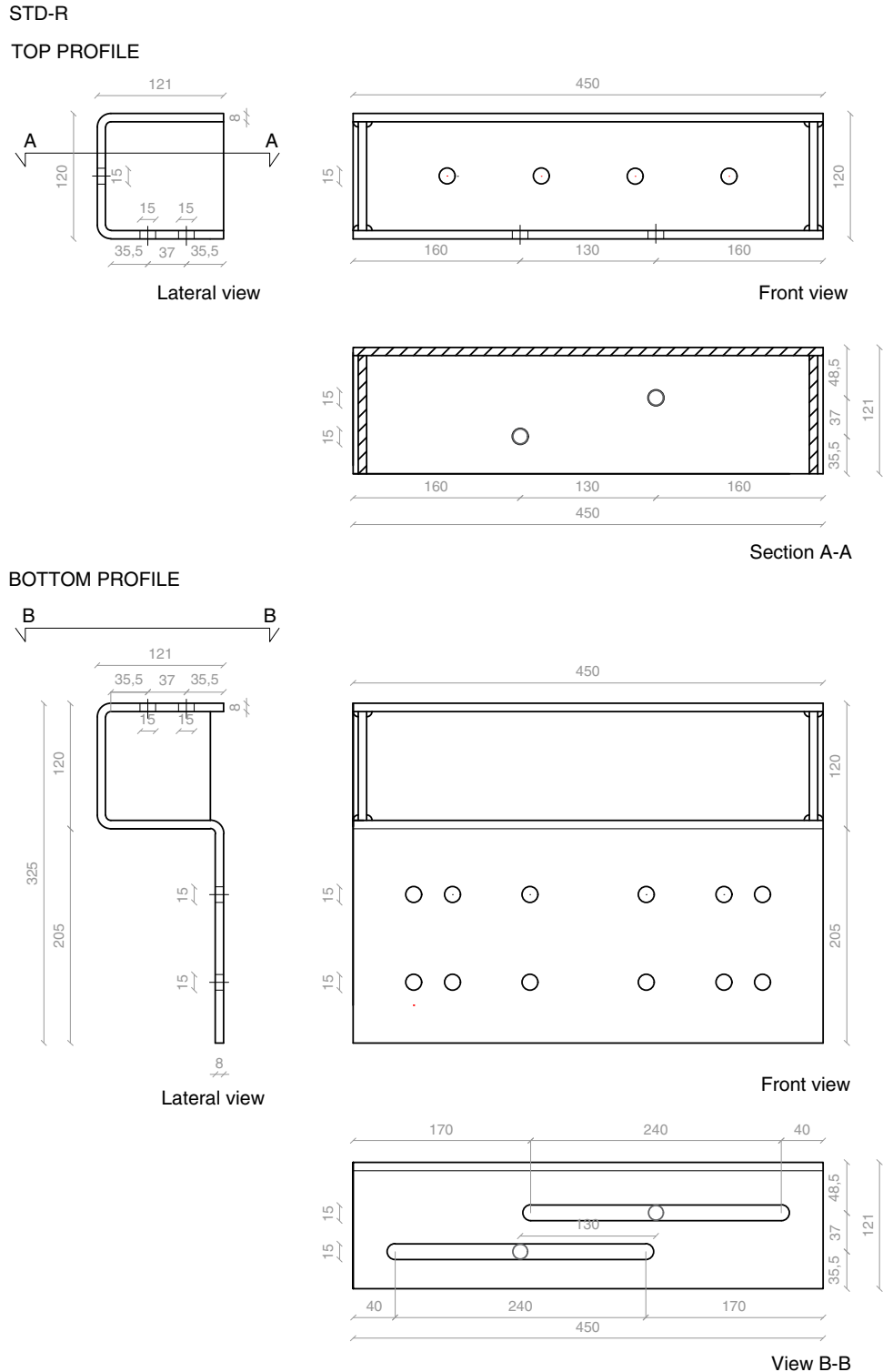

Fig. 19. STD-R specimen, measurements in millimeters.

geometry: the eccentricity and the number of bends. As future work, the authors aim at expanding the experimental campaign by investigating the issues that arose during the current campaign: choice of different structural arrangements, use of different materials as shim layers with higher hardness than steel, and developing hysteresis models for the complete e-CLT system (Aloisio et al. 2022a, b).

Appendix. Technical Drawings

This section provides the technical drawings of the tested specimen, which include the details on the measure and locations of the holes for the sliding movement. Fig. 18 shows a technical drawing of the STD specimen, Fig. 19 of the STD-R specimen, Fig. 20 of the STD-1H specimen, and Fig. 21 of the ALT specimen.
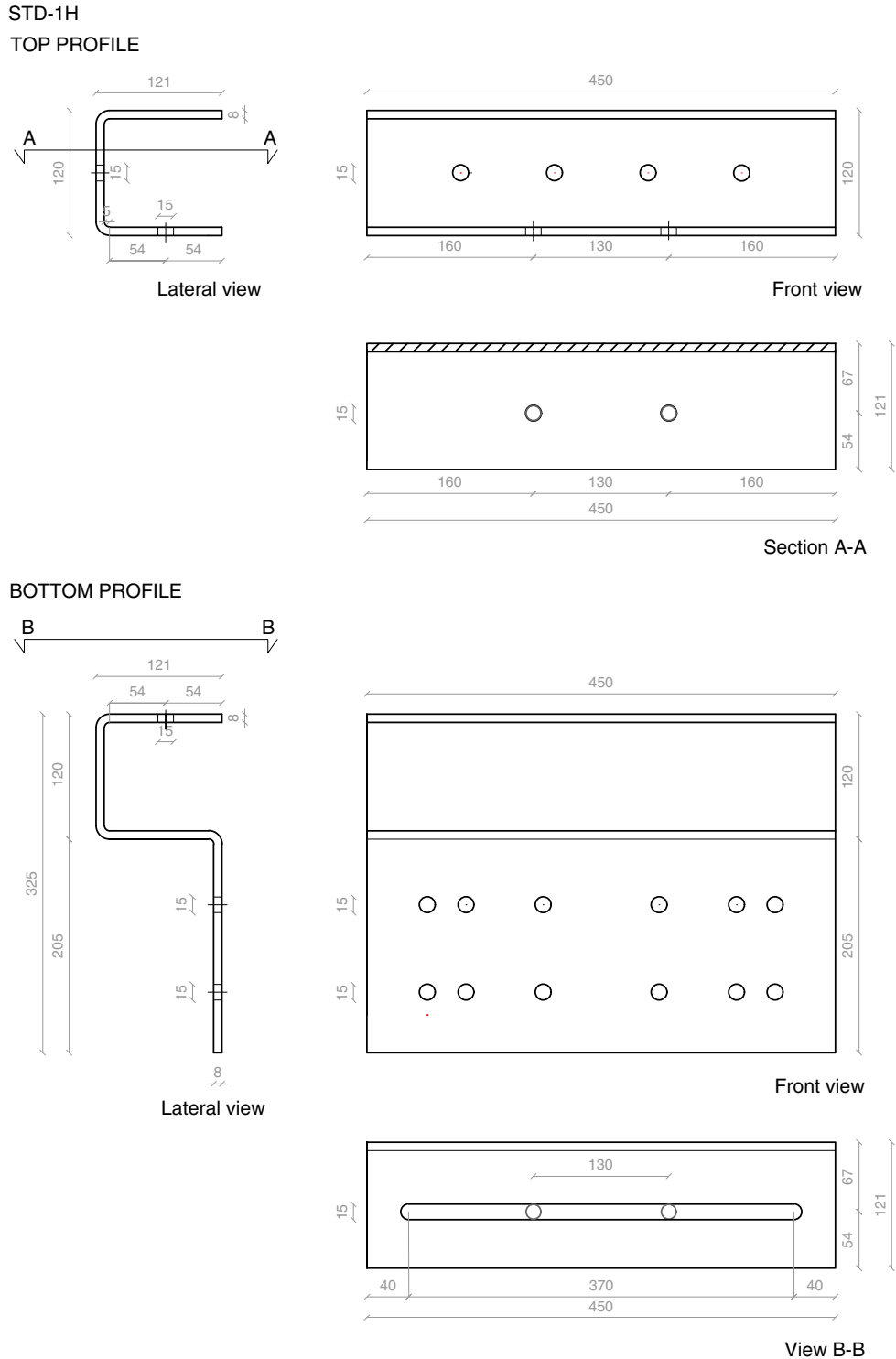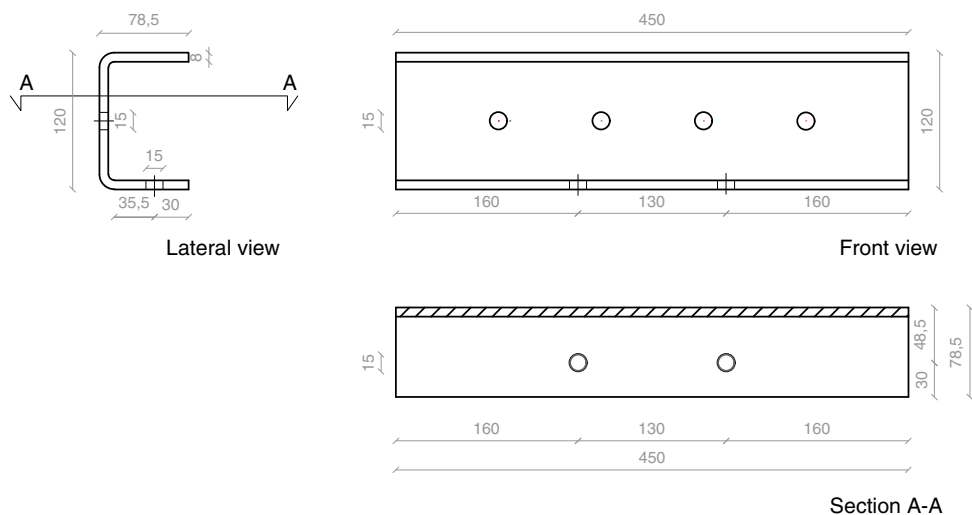

Fig. 20. STD-1H specimen, measurements in millimeters.

ALT
TOP PROFILE

Lateral view

Front view

Section A-A

BOTTOM PROFILE

Lateral view
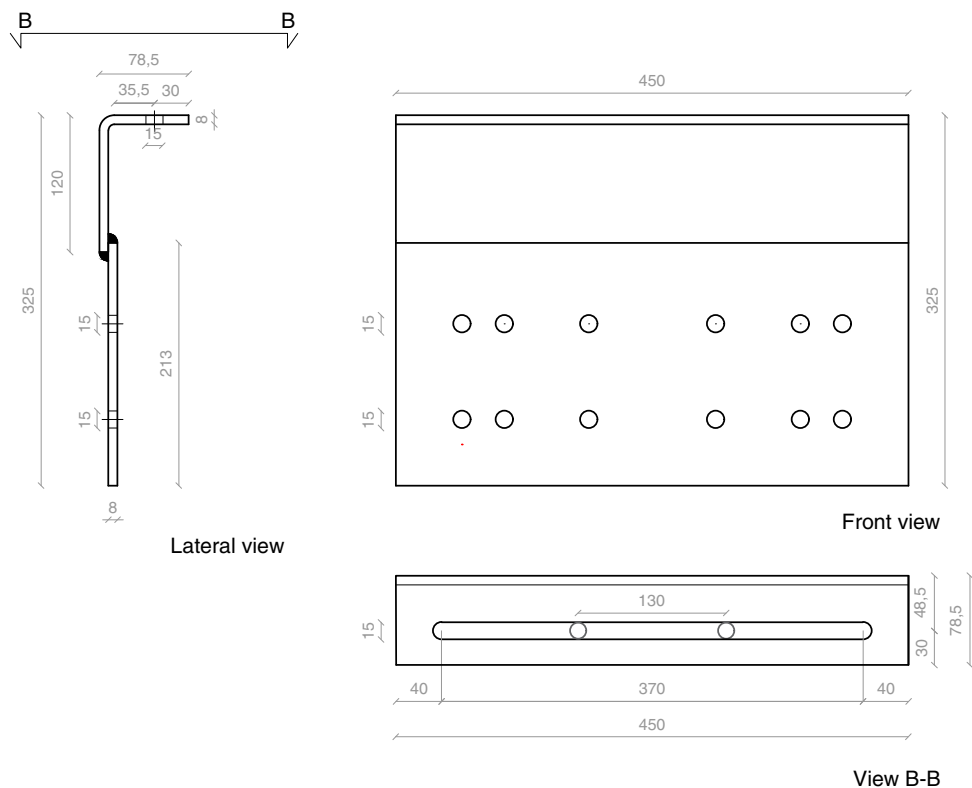
Front view

View B-B

Fig. 21. ALT specimen, measurements in millimeters.

Data Availability Statement

Some or all data, models, or code that support the findings of this study are available from the corresponding author upon reasonable request.

Acknowledgments

References

Aloisio, A., F. Boggian, and R. Tomasi. 2022a. "Design of a novel seismic retrofitting system for RC structures based on asymmetric friction connections and CLT panels." *Eng. Struct.* 254 (4): 113807. https://doi.org/10.1016/j.engstruct.2021.113807.

Aloisio, A., M. Pelliciari, S. Sirotti, F. Boggian, and R. Tomasi. 2022b. "Optimization of the structural coupling between RC frames, CLT shear walls and asymmetric friction connections." *Bull Earthq. Eng.* https://doi.org/10.1007/s10518-022-01337-8.

Barbagallo, F., M. Bosco, E. M. Marino, P. P. Rossi, and P. R. Stramondo. 2017a. "A multi-performance design method for seismic upgrading of existing RC frames by BRBS." *Earthquake Eng. Struct. Dyn.* 46 (7): 1099–1119. https://doi.org/10.1002/eqe.2846.

Barbagallo, F., I. Hamashima, H. Hu, M. Kurata, and M. Nakashima. 2017b. "Base shear capping buildings with graphite-lubricated bases for collapse prevention in extreme earthquakes." *Earthquake Eng. Struct. Dyn.* 46 (6): 1003–1021. https://doi.org/10.1002/eqe.2842.

Björnfot, A., F. Boggian, A. Nygård, and R. Tomasi. 2017. "Strengthening of traditional buildings with slim panels of cross-laminated timber (CLT)." In *Proc., Int. Conf. on Structural Health Assessment of Timber Structures*. Guimarães, Portugal: Univ. of Minho.

Borzouie, J., G. A. MacRae, J. G. Chase, G. W. Rodgers, and G. C. Clifton. 2016. "Experimental studies on cyclic performance of column base strong axis–aligned asymmetric friction connections." *J. Struct. Eng.* 142 (1): 04015078. https://doi.org/10.1061/(ASCE)ST.1943-541X.0001327.

Bournas, D. A., T. C. Triantafillou, K. Zygouris, and F. Stavropoulos. 2009. "Textile-reinforced mortar versus FRP jacketing in seismic retrofitting of RC columns with continuous or lap-spliced deformed bars." *J. Compos. Constr.* 13 (5): 360–371. https://doi.org/10.1061/(ASCE)CC.1943-5614.0000028.

Caterino, N., I. Iervolino, G. Manfredi, and E. Cosenza. 2008. "Multi-criteria decision making for seismic retrofitting of RC structures." *J. Earthquake Eng.* 12 (4): 555–583. https://doi.org/10.1080/13632460701572872.

CEN (European Committee for Standardization). 2018a. *Anti-seismic devices*. EN 15129. Brussels, Belgium: CEN.

CEN (European Committee for Standardization). 2018b. *Execution of steel structures and aluminium structures—Part 2: Technical requirements for steel structures*. EN 1090-2. Brussels, Belgium: CEN.

Chanchi Golondrino, J. C., G. A. MacRae, J. G. Chase, G. W. Rodgers, and G. C. Clifton. 2018. "Hysteretic behaviour of asymmetrical friction connections using brake pads of d3923." *Structures* 16 (Nov): 164–175. https://doi.org/10.1016/j.istruc.2018.09.012.

Chanchi Golondrino, J. C., G. A. MacRae, J. G. Chase, G. W. Rodgers, and G. C. Clifton. 2019. "Asymmetric friction connection (AFC) design for seismic energy dissipation." *J. Constr. Steel Res.* 157 (Jun): 70–81. https://doi.org/10.1016/j.jcsr.2019.02.027.

Chanchi Golondrino, J. C., G. A. MacRae, J. G. Chase, G. W. Rodgers, and G. C. Clifton. 2020. "Seismic behaviour of symmetric friction connections for steel buildings." *Eng. Struct.* 224 (Dec): 111200. https://doi.org/10.1016/j.engstruct.2020.111200.

Clemente, P., and G. Buffarini. 2010. "Base isolation: Design and optimization criteria." *Seismic Isolation Protect. Syst.* 1 (1): 17–40. https://doi.org/10.2140/siaps.2010.1.17.

Del Vecchio, C., M. Di Ludovico, A. Balsamo, A. Prota, G. Manfredi, and M. Dolce. 2014. "Experimental investigation of exterior RC beam-column joints retrofitted with FRP systems." *J. Compos. Constr.* 18 (4): 04014002. https://doi.org/10.1061/(ASCE)CC.1943-5614.0000459.

Di Ludovico, M., A. Prota, C. Moroni, G. Manfredi, and M. Dolce. 2017. "Reconstruction process of damaged residential buildings outside historical centres after the L'aquila earthquake: Part I—'Light damage' reconstruction." *Bull. Earthquake Eng.* 15 (2): 667–692. https://doi.org/10.1007/s10518-016-9877-8.

Di Sarno, L., and G. Manfredi. 2010. "Seismic retrofitting with buckling restrained braces: Application to an existing non-ductile RC framed building." *Soil Dyn. Earthquake Eng.* 30 (11): 1279–1297. https://doi.org/10.1016/j.soildyn.2010.06.001.

Dubey, R., and P. Kumar. 2016. "Experimental study of the effectiveness of retrofitting rc cylindrical columns using self-compacting concrete jackets." *Constr. Build. Mater.* 124 (Oct): 104–117. https://doi.org/10.1016/j.conbuildmat.2016.07.079.

e-SAFE. n.d. "Energy and seismic affordable renovation solutions." Accessed March 23, 2021. http://esafe-buildings.eu/.

Fitzgerald, D., T. Miller, A. Sinha, and J. Nairn. 2020. "Cross-laminated timber rocking walls with slip-friction connections." *Eng. Struct.* 220 (Oct): 110973. https://doi.org/10.1016/j.engstruct.2020.110973.

Fitzgerald, D., A. Sinha, T. H. Miller, and J. A. Nairn. 2021. "Axial slip-friction connections for cross-laminated timber." *Eng. Struct.* 228 (Feb): 111478. https://doi.org/10.1016/j.engstruct.2020.111478.

Golondrino, J., G. MacRae, J. Chase, and G. Rodgers. 2012a. "Behaviour of asymmetrical friction connections using different shim materials." In *Proc., New Zealand Society for Earthquake Engineering Conf.* Wellington, New Zealand: New Zealand Society for Earthquake Engineering.

Golondrino, J., G. MacRae, J. Chase, G. Rodgers, and C. Clifton. 2012b. "Clamping force effects on the behaviour of asymmetrical friction connections (AFC)." In *Proc., 15th World Conf. on Earthquake Engineering*. Red Hook, NY: Curran Associates.

Golondrino, J., G. MacRae, J. Chase, G. Rodgers, and C. Clifton. 2016. "Effects of the bolt grip length on the behaviour of asymmetrical friction connections (AFC)." In *Proc., New Zealand Society for Earthquake Engineering Conf.* Wellington, New Zealand: New Zealand Society for Earthquake Engineering.

Golondrino, J. C. C., G. A. MacRae, J. G. Chase, G. W. Rodgers, and G. C. Clifton. 2020. "Asymmetric friction connection bolt lever arm effects on hysteretic behaviour." *J. Earthquake Eng.* 1–22. https://doi.org/10.1080/13632469.2020.1733136.

Hatletveit, M. R. 2020. "Mechanical assessment of a steel dissipating system for RC buildings retrofitting with CLT panels." M.S. thesis, Faculty of Science and Technology, Norwegian Univ. of Life Sciences.

Horizon. 2020. "Reducing energy consumption and carbon footprint by smart and sustainable use." Accessed March 23, 2021. https://cordis.europa.eu/project/id/893135.

ISO. 2003. *Timber structures: Joints made with mechanical fasteners–Quasi-static reversed-cyclic test method*. ISO 16670. Geneva, Switzerland: ISO.

Istat (Istituto Nazionale di Statistica). 2015. *Annuario Statistico Italiano*. Rome: Istituto nazionale di statistica.

Jaisee, S., F. Yue, and Y. H. Ooi. 2021. "A state-of-the-art review on passive friction dampers and their applications." *Eng. Struct.* 235 (May): 112022. https://doi.org/10.1016/j.engstruct.2021.112022.

Javadi, P., A. Tizchang, A. GhafourianHesami, and M. Askari. 2020. "A friction-based connection for retrofitting RC frames by steel braced frames." *Structures* 24 (Apr): 627–639. https://doi.org/10.1016/j.istruc.2019.12.021.

Khoo, H.-H., C. Clifton, J. Butterworth, and G. MacRae. 2013. "Experimental study of full-scale self-centering sliding hinge joint connections with friction ring springs." *J. Earthquake Eng.* 17 (7): 972–997. https://doi.org/10.1080/13632469.2013.787378.

Khoo, H.-H., C. Clifton, G. MacRae, H. Zhou, and S. Ramhormozian. 2015. "Proposed design models for the asymmetric friction connection." *Earthquake Eng. Struct. Dyn.* 44 (8): 1309–1324. https://doi.org/10.1002/eqe.2520.

Latour, M., G. Rizzano, A. Santiago, and L. S. da Silva. 2019. "Experimental response of a low-yielding, self-centering, rocking column base joint with friction dampers." *Soil Dyn. Earthquake Eng.* 116 (Jan): 580–592. https://doi.org/10.1016/j.soildyn.2018.10.011.

Loo, W., P. Quenneville, and N. Chouw. 2014a. "A new type of symmetric slip-friction connector." *J. Constr. Steel Res.* 94 (Mar): 11–22. https://doi.org/10.1016/j.jcsr.2013.11.005.

Loo, W. Y., C. Kun, P. Quenneville, and N. Chouw. 2014b. "Experimental testing of a rocking timber shear wall with slip-friction connectors." *Earthquake Eng. Struct. Dyn.* 43 (11): 1621–1639. https://doi.org/10.1002/eqe.2413.

Loo, W. Y., P. Quenneville, and N. Chouw. 2012. "A numerical study of the seismic behaviour of timber shear walls with slip-friction connectors."

Eng. Struct. 34 (Jan): 233–243. https://doi.org/10.1016/j.engstruct.2011 .09.016.

Loo, W. Y., P. Quenneville, and N. Chouw. 2014c. "A new type of symmetric slip-friction connector." *J. Constr. Steel Res.* 94 (Mar): 11–22. https://doi.org/10.1016/j.jcsr.2013.11.005.

Loo, W. Y., P. Quenneville, and N. Chouw. 2016. "Rocking timber structure with slip-friction connectors conceptualized as a plastically deformable hinge within a multistory shear wall." *J. Struct. Eng.* 142 (4): E4015010. https://doi.org/10.1061/(ASCE)ST.1943-541X.0001387.

Loo, W. Y., P. Quenneville, and N. Chouw. 2017. "The influence of surface preparation and the lubricating effect of mill scale on the performance of slip-friction connectors." *Constr. Build. Mater.* 155 (Nov): 1025–1038. https://doi.org/10.1016/j.conbuildmat.2017.08.100.

Margani, G., G. Evola, C. Tardo, and E. M. Marino. 2020. "Energy, seismic, and architectural renovation of RC framed buildings with prefabricated timber panels." *Sustainability* 12 (12): 4845. https://doi.org/10.3390 /su12124845.

Marthinsen, M. B. A. 2020. "Experimental assessment of a steel dissipating system." M.S. thesis, Faculty of Science and Technology, Norwegian Univ. of Life Sciences.

Pantazopoulou, S. J., S. P. Tastani, G. E. Thermou, T. Triantafillou, G. Monti, D. Bournas, and M. Guadagnini. 2016. "Background to the European seismic design provisions for retrofitting RC elements using FRP materials." *Struct. Concr.* 17 (2): 194–219. https://doi.org/10.1002 /suco.201500102.

Rad, A. A., G. A. MacRae, N. K. Hazaveh, and Q. Ma. 2019. "Shake table testing of a low damage steel building with asymmetric friction connections (AFC)." *J. Constr. Steel Res.* 155 (Apr): 129–143. https://doi.org /10.1016/j.jcsr.2018.12.013.

Rahimi, A., and M. R. Maheri. 2018. "The effects of retrofitting RC frames by X-bracing on the seismic performance of columns." *Eng.*

Struct. 173 (Oct): 813–830. https://doi.org/10.1016/j.engstruct.2018 .07.003.

Rahimi, A., and M. R. Maheri. 2020. "The effects of steel x-brace retrofitting of RC frames on the seismic performance of frames and their elements." *Eng. Struct.* 206 (Mar): 110149. https://doi.org/10.1016/j .engstruct.2019.110149.

Rodgers, G. W., R. Herve, G. A. MacRae, J. Chanchi Golondrino, and J. G. Chase. 2018. "Dynamic friction coefficient and performance of asymmetric friction connections." In Vol. 14 of *Structures*, 416–423. Amsterdam, Netherlands: Elsevier. https://doi.org/10.1016/j.istruc.2017.09.003.

SBE-Varvit. 2021. "Structural bolting assemblies: EN 14399: Preloaded assemblies." Accessed September 11, 2021. https://secure.varvit.com /pdf/EN14399.pdf.

Stazi, F., M. Serpilli, G. Maracchini, and A. Pavone. 2019. "An experimental and numerical study on CLT panels used as infill shear walls for RC buildings retrofit." *Constr. Build. Mater.* 211 (Jun): 605–616. https://doi .org/10.1016/j.conbuildmat.2019.03.196.

Sustersic, I., and B. Dujic. 2013. "Seismic strengthening of existing URM and RC structures using XLAM timber panels." In *Proc., Int. Conf. on Earthquake Engineering*. Berlin: Springer.

TahamouliRoudsari, M., M. B. Eslamimanesh, A. Entezari, O. Noori, and M. Torkaman. 2018. "Experimental assessment of retrofitting RC moment resisting frames with ADAS and TADAS yielding dampers." In Vol. 14 of *Structures*, 75–87. Amsterdam, Netherlands: Elsevier. https://doi.org/10.1016/j.istruc.2018.02.005.

Tardo, C., F. Boggian, M. Hatletveit, E. Marino, G. Margani, and R. Tomasi. 2020. "Mechanical characterization of energy dissipation devices in retrofit solution of reinforced concrete frames coupled with solid wood panels." In *Proc., 12th Int. Conf. on Structural Analysis of Historical Constructions*. Ås, Norway: Norwegian Univ. of Life Sciences.